Polymer 49 (2008) 2520–2530

Contents lists available at ScienceDirect

Polymer

journal homepage: www.elsevier.com/locate/polymer

In situ preparation and continuous fiber spinning of poly(*p*-phenylene benzobisoxazole) composites with oligo-hydroxyamide-functionalized multi-walled carbon nanotubes

Chengjun Zhou [a], Shanfeng Wang [b,*], Yi Zhang [c], Qixin Zhuang [a,**], Zhewen Han [a]

[a] *Key Laboratory for Ultrafine Materials of Ministry of Education, School of Materials Science and Engineering, East China University of Science and Technology, Shanghai 200237, China*
[b] *Department of Materials Science and Engineering, The University of Tennessee, Knoxville, TN 37996, USA*
[c] *State Key Laboratory for Modification of Chemical Fibers and Polymer Materials, Donghua University, Shanghai 200051, China*

ARTICLE INFO

Article history:
Received 24 January 2008
Received in revised form 31 March 2008
Accepted 2 April 2008
Available online 8 April 2008

Keywords:
Carbon nanotubes
Polybenzazoles
Nanocomposites

ABSTRACT

A graft-from approach has been performed to achieve covalent functionalization of multi-walled carbon nanotubes (MWNTs) with oligo-hydroxyamide (oHA). Pristine MWNT was first oxidized to MWNT-COOH and then functionalized to MWNT-COCl by acyl chloride. MWNT-COCl was copolymerized with oHA to produce oHA-grafted MWNTs (MWNT-oHA). The thickness of the oHA shell in MWNT-oHA is about 7.5 nm. MWNT-oHA has a remarkable solubility in polar solvents and a good thermal stability because characteristic dehydrative ring closure occurs upon heating and forms a thermally more stable benzoxazole component. MWNT-oHA has been further covalently incorporated with a rigid-rod polymer matrix, poly(*p*-phenylene benzobisoxazole) (PBO), through in situ polymerization. Continuous PBO–MWNT composite fibers with different MWNT compositions have been fabricated using dry-jet wet-spinning technique. The structure and morphology of PBO–MWNT composite fibers have been characterized and their mechanical, thermal, conducting properties have been investigated. The tensile modulus, tensile strength, and thermal stability of PBO–MWNT composite fibers have been improved because of a good dispersion and high alignment of MWNTs in PBO as well as enhanced interfacial interaction between these two components. Furthermore, increased conductivity has been discovered in the PBO–MWNT composite films and the inner core of the composite fibers; however, not on the outer surface. The phenomena can be interpreted using percolation model together with the heterogeneous fiber morphology and nanotube distribution over the cross-section of the fiber.

1. Introduction

Since carbon nanotubes (CNTs) were first reported by Iijima in 1991 [1], they have attracted tremendous attention because of their excellent electrical and superior mechanical properties [2,3]. Diverse applications based on this unique material have been proposed. Particularly, polymer–CNT composites have been pursued with the hope of delivering CNTs' properties to a processable and synergistic host material. To date, a variety of polymers have been used to prepare polymer–CNT composites for different targeting applications [4–22].

However, owing to their rigidity and chemical inertness, CNTs are difficult to dissolve or disperse in common organic solvents or polymeric matrices for making useful articles. Great efforts have been focused on applying the methods of covalent or non-covalent functionalization to improve the solubilization of CNTs [7–22]. Covalent functionalization also provides a means for engineering the CNT–polymer interface to achieve optimal composite properties [10–22]. With respect to mechanical properties, enhanced interfacial adhesion and maximized load transfer could be accomplished through covalent or non-covalent interactions between the functional groups on the nanotubes and polymer matrix [9].

In the present study, we report a covalent modification of multi-walled carbon nanotubes (MWNTs) using a low-molecular-weight polyhydroxyamide (PHA) or oligo-hydroxyamide (oHA) to improve the solubility, dispersivity, and interfacial adhesion of MWNTs in polymer matrix. More importantly, this method can be used to explore the potentials of MWNTs in fabricating macroscopic functional articles such as high-performance fibers or films. PHA can form a thermally more stable polymer, poly(*p*-phenylene benzobisoxazole) (PBO), through further ring closure in polycondensation at elevated temperature [23–29]. Although many polymer–CNT

* Corresponding author. Tel.: +1 865 974 7809; fax: +1 865 974 4115.
** Corresponding author. Tel.: +86 21 6425 3060.
E-mail addresses: swang16@utk.edu (S. Wang), qxzhuang@ecust.edu.cn (Q. Zhuang).

0032-3861/$ – see front matter © 2008 Elsevier Ltd. All rights reserved.
doi:10.1016/j.polymer.2008.04.003

composites including a few PBO–CNT composites have been reported [30–34], the improvement in electrical conductivity has not yet been achieved. The earlier reported PBO–CNT composites were prepared using in situ polymerization of PBO with pristine CNTs or carboxylated CNTs [30–32,34], or solution blending of PBO and MWNTs [33].

Our approach in this report is to prepare a series of PBO–MWNT composites at different compositions of MWNT (ϕ_{MWNT}) using in situ polymerization of PBO in the presence of this novel oHA-functionalized MWNT (MWNT-oHA). Moreover, long, continuous composite fibers have been fabricated using dry-jet wet-spinning technique. The dispersion, orientation, and interfacial adhesion of CNTs in the PBO–MWNT composite fibers have been characterized for understanding the effects of oHA-grafted MWNTs on the morphological, thermal, mechanical, and electrical properties of PBO–MWNT composites.

2. Experimental

2.1. Materials

One monomer for polymerizing PBO, 4,6-diaminoresorcinol dihydrochloride (DAR·2HCl), was synthesized in our laboratory according to the previous reports [35–41]. Another monomer terephthalic acid (TPA) was purchased from Shanghai Reagents Co. and ground to powder in a glove box prior to use. Methanesulfonic acid (MSA) was purchased from Sigma–Aldrich Chemical Co. Terephthalic chloride (TPC), polyphosphoric acid (PPA), dimethyl acetamide (DMAc), *N*-methyl-2-pyrrolidone (NMP), thionyl chloride ($SOCl_2$), pyridine, acetone, tetrahydrofuran (THF), and other chemicals were also purchased from Shanghai Reagents Co. The low-boiling-point organic solvents were distilled and kept in the presence of 4 Å molecular sieves to eliminate water. MWNT was provided from Tsinghua-Nafine Nano-Powder commercialization engineering center in Beijing, China.

2.2. Preparation of acyl chloride MWNT (MWNT-COCl)

A typical procedure (Scheme 1) of preparing MWNT-COCl is described as follows. The first step was to attach carboxyl groups onto the surface of nanotubes. In this carboxylation procedure, 1.5 g of pristine MWNT was added to 30.0 mL of 65% HNO_3 aqueous solution. The mixture was treated with ultrasonic bath (40 kHz) for 30 min, and then stirred for 20 h in reflux at 90 °C. After that, the mixture was filtered through a 0.2 μm millipore polycarbonate membrane, and washed with excess distilled water until no residual acid was present. The filtered solid was dried under vacuum for 12 h at 60 °C. Three hundred milligrams of the obtained MWNT-COOH was suspended in 20 mL of $SOCl_2$. The suspension was stirred at 70 °C for 24 h to convert the surface-bound carboxyl groups into acyl chloride groups. The solid was then filtered and washed with anhydrous THF. Subsequently it was dried under vacuum at room temperature for 2 h.

2.3. Synthesis of oligo-hydroxyamide (oHA)

A typical procedure for synthesizing oHA is illustrated in Scheme 2 and it proceeded as follows [23–27]. To a 100 mL three-neck round-bottom flask equipped with a nitrogen inlet, a mechanical stirrer and a condenser, 0.36 g (1.7 mmol) of DAR·2HCl, 0.54 g (6.8 mmol) of pyridine and 20 g of anhydrous NMP were added. The solution was stirred until it became homogeneous and then cooled to 5 °C in ice water. Then 0.34 g (1.68 mmol) of TPC was added dropwise to the solution and reacted at room temperature for 16 h. The resulted viscous solution was precipitated in 300 mL of deionized water. Precipitated oHA was collected by filtration and washed with methanol before it was dried under vacuum at 60 °C for 24 h. The intrinsic viscosity of oHA was 0.2 dL g^{-1} measured in NMP at a concentration of 0.5 g dL^{-1} at 30 °C. Anal. Calcd for oHA $(C_{14}O_4H_{10}N_2)_n$: C, 62.22; H, 3.70; N, 10.37. Found: C, 61.23; H, 3.86; N, 10.98.

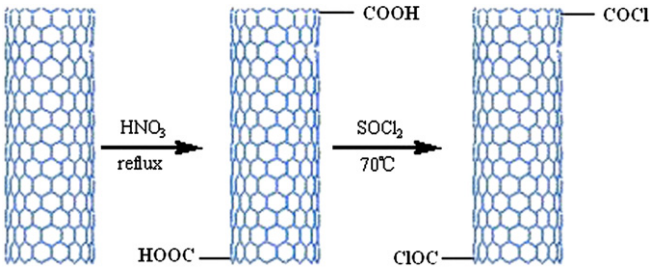

Scheme 1. Synthesis of MWNT-COCl.

2.4. Synthesis of oligo-HA-grafted MWNT (MWNT-oHA)

A typical procedure for synthesizing MWNT-oHA from MWNT-COCl and oHA is depicted in Scheme 3. Similar to the synthesis of oHA, 0.3 g of newly prepared oHA, 0.2 g of pyridine and 20 g of anhydrous NMP were added to a 100 mL three-neck round-bottom flask equipped with a nitrogen inlet, a mechanical stirrer, and a condenser. The solution was stirred until it became homogeneous and then cooled to 5 °C in ice water. Ten milliliters of MWNT-COCl/NMP solution with a concentration of 0.01 g/ml, dispersed with ultrasonic bath (40 kHz) for 30 min, was injected using a syringe dropwise into the flask. Then the reacting solution was stirred at room temperature for 16 h. MWNT-oHA was precipitated in water and filtered using a 0.45 μm PTFE filter. After being washed with excess water and acetone, MWNT-oHA was dried under vacuum at 100 °C.

2.5. In situ polymerization of PBO–MWNT composites

Viscous solutions of PBO or its composites with MWNT in PPA were prepared using the polycondensation [28,35–41] of DAR·2HCl and TPA without or with MWNTs-oHA. A typical procedure for preparing PBO–MWNT composite shown in Scheme 4, is as follows: 10 g of DAR·2HCl, 7.797 g of TPA, and 40.3 g of PPA were loaded into a 250 mL glass vessel equipped with a mechanical stirrer and nitrogen inlet/outlet. The mixture was stirred at 90 °C under a nitrogen atmosphere until complete removal of hydrochloride. Another 29.9 g of P_2O_5 and MWNT-oHA were then added to the mixture to bring the P_2O_5 concentration up to 85 wt% and result in a final polymer concentration of 14 wt%. The polymerizing mixture was first stirred under vacuum at 120 °C for 8 h. It was then heated to 180 °C stepwise at 5–10 °C h^{-1}, and kept at this temperature for

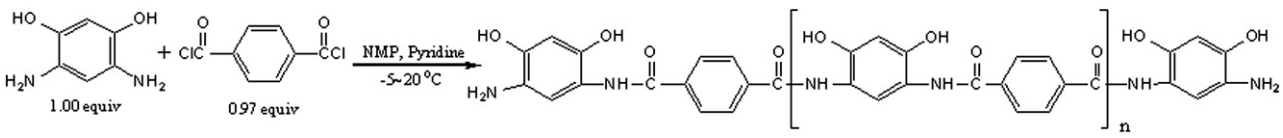

Scheme 2. Synthesis of oHA.

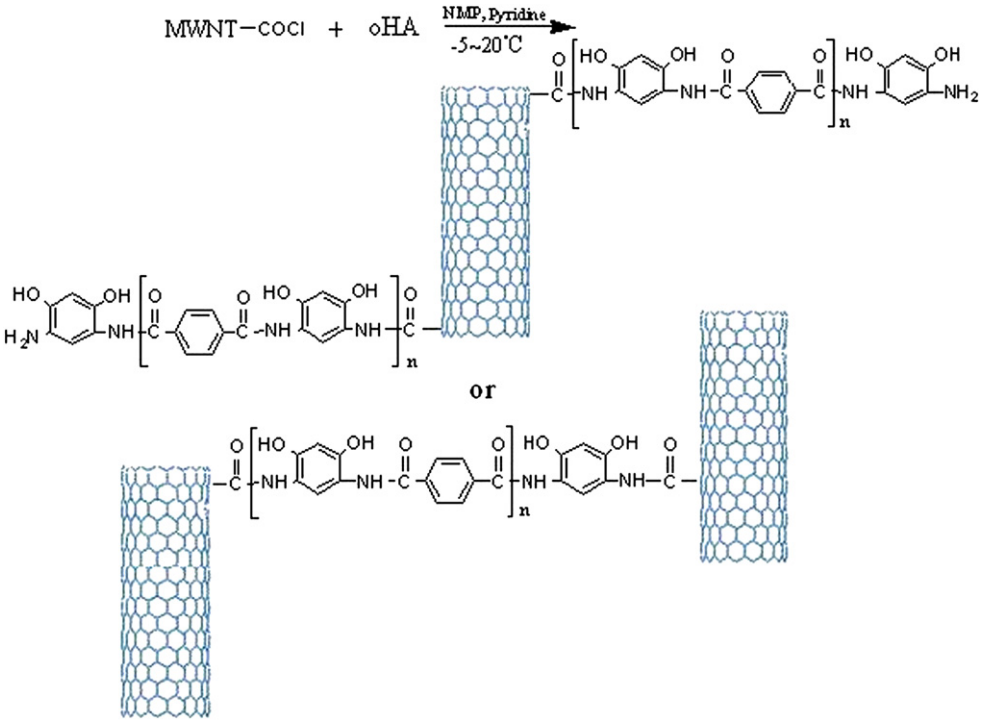

Scheme 3. Synthesis of MWNT-oHA.

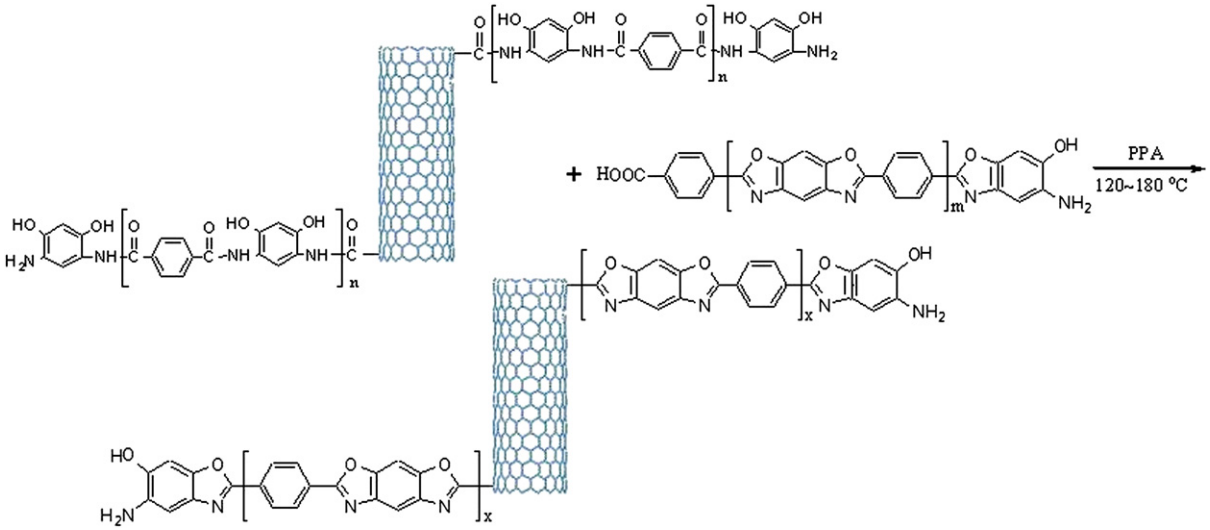

Scheme 4. In situ polymerization of PBO–MWNT composite.

another 8 h with constant stirring. MWNT compositions were 0.18, 0.36, and 0.54 wt% with respect to the polymer concentrations in the polymerization.

2.6. Fabrication of PBO–MWNT composite fibers

Using the freshly synthesized PBO or PBO–MWNT viscous solutions in PPA with a PBO or PBO–MWNT concentration of 14 wt%, their fibers were drawn by the dry-jet wet-spinning technique [28] on a lab-scale spinneret assembly as illustrated in Fig. 1. PBO or PBO–MWNT composite dope was first transferred under the protection of a nitrogen atmosphere to the dope tank and was heated at 160 °C for ~3 h before spinning. Then the dope tank was pressurized with nitrogen (2 MPa) to extrude the dope through the spinneret with a diameter of 1 mm. The composite fiber solidified as it

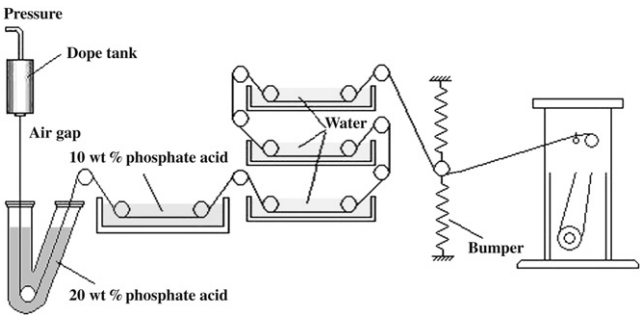

Fig. 1. Fabrication of PBO and PBO–MWNT composite fibers using dry-jet wet-spinning technique.

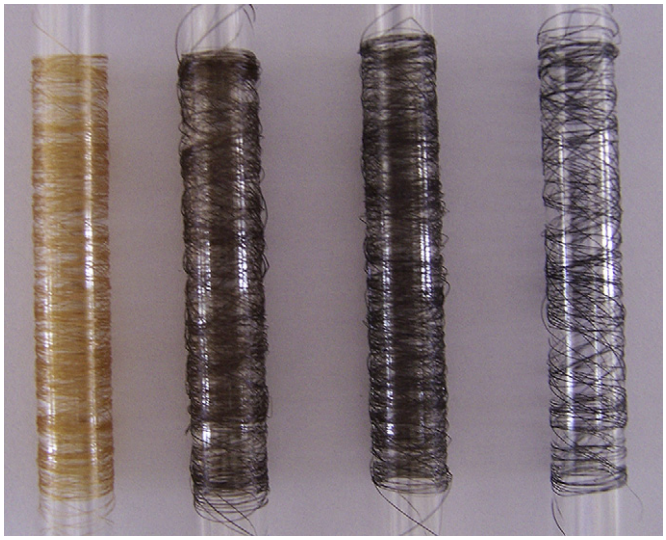

Fig. 2. Photograph of PBO and PBO–MWNT composite continuous fibers collected using spools. The MWNT composition increases from left to right, namely, 0, 0.18, 0.36, and 0.54 wt%.

was cooled along a 20-cm-long air gap and coagulated in a bath of phosphate acid. The solvent PPA in fibers was washed with water at room temperature. A typical fiber diameter is approximately 60 μm, and thus the draw ratio in fabrication is 16 as calculated from the ratio of spinneret exit diameter and fiber diameter. Fibers wrapped on plastic spools were dried with running air for three days. Dried fibers were further heat-treated at 460 °C in nitrogen for 1 min with a tension of 20 MPa applied on the fibers. The process allowed the facile fabrication of continuous black, shining PBO–MWNT fibers as shown together with golden PBO fibers in Fig. 2.

2.7. Structural characterizations

Elemental analysis was carried out with an elementary analyzer (Elementar Vario EL-III). Fourier-transform infrared (FTIR) spectra of pristine MWNTs, oHA, and MWNTs-oHA were obtained on a Nicolet FTIR analyzer (Magna-IR550) with KBr disks. Transmission FTIR spectra of nanocomposites were obtained using sample-spread CaF_2 disks. Raman spectra were collected at 514 nm excitation (He–Ne laser) on a Renishaw InVia Reflex Raman spectrometer in a back-scattering configuration. MWNT and MWNT-oHA were examined with a JEOL JEM-1200EX-II transmission electron microscope (TEM) at 200 kV, and the samples were prepared by placing one drop of suspension or solution on copper grids coated with carbon. Wide-angle X-ray diffraction (WAXD) patterns of PBO and PBO–MWNT composite fibers were obtained on a multi-filament bundle by the D/Max-2550 PC rotating anode X-ray generator with Ni-filtered Cu Kα radiation operated at 350 mA and 40 kV. Dispersion of MWNTs into PBO matrix was assessed using a JEOL JSM-6360LV scanning electron microscope (SEM).

2.8. Measurements

Thermal gravimetric analysis (TGA) was carried out on a DuPont 1090B thermal gravimetric analyzer with a heating rate of 10 °C min^{-1} in the nitrogen flow (20 mL min^{-1}). Photos of MWNTs-oHA placed in different solvents were taken using a digital camera (Kodak, DSC-Z730). The mechanical properties of PBO and PBO–MWNT composite fibers were measured at 25 °C with a YG020C brute force machine (Shuang-gu Textile Instrument Co., Changzhou, China) at a displacement rate of 20 mm min^{-1}. For each sample, 10 specimens were measured and averaged. The room temperature electrical resistivity ρ in Ω cm of the fibers was measured between a distance of 1 cm along the longitudinal direction of the fibers using a ZC36 high resistance electrometer (Shanghai Cany Precision Instrument Co., Ltd) with direct current after equilibrium of 2 min. Electric glue was used to ensure a good contact between the fiber and the copper line. In order to investigate the electrical conductivity in the fiber core, PBO and PBO–MWNT fibers were split into symmetrical halves using a blade and the measurement was done on the fiber core using the same method. The electrical resistivity of PBO and PBO–MWNT films was measured at room temperature using a Mastech-my61 picoammeter (Precision Mastech Enterprises Co., China) in the perpendicular direction of the molded sheets. Silver paste was used to ensure a good contact between sample surface and copper electrodes. In the following discussion, the conductivity σ in S cm^{-1} was calculated from ρ using the equation $\rho = 1/\sigma$.

3. Results and discussion

3.1. Characterization and properties of MWNT-oHA

Fig. 3 shows the ATR-IR spectra of MWNT-COOH, oHA, and MWNT-oHA. The C═O and –OH stretching modes of the carboxyl group at 1705 and 3100–3700 cm^{-1}, and C═C graphitic stretch in MWNTs at 1560 cm^{-1} can be observed in the spectrum of MWNT-COOH [15–22]. Oligo-HA exhibits a broad absorption band at 3200–3600 cm^{-1} due to amino (N–H) and hydroxyl (–OH) groups, and strong amide carbonyl absorption at 1650 cm^{-1}. The absorption peaks at ~1370 cm^{-1} in the spectrum of oHA can be assigned to the C–N stretch. In addition, the absence of carbonyl group in –COOH clearly shows that oHA was end-capped with DAR groups. In the spectrum of MWNT-oHA, the small peaks at 1700 cm^{-1} can be assigned to unreacted C═O in MWNT-COCl that confirms the existence of MWNT in MWNT-oHA. The C═O peak intensity at 1650 cm^{-1} significantly increases after the functionalization, suggesting the covalent bonding between MWNT and oHA. The peaks at ~1530 and ~1460 cm^{-1} can be assigned to the aromatic ring C═C stretch in oHA attached to MWNTs and overlapping with the C═C graphitic stretch in MWNTs.

As mentioned in Section 2, the elemental analysis result of oHA is consistent with its theoretical compositions for oHA with five repeating units approximately. As a result, its average molecular weight is 1764 g/mol. Elemental analysis was also employed to determine the MWNT composition in MWNT-oHA using the content of nitrogen as a standard with the later confirmation by

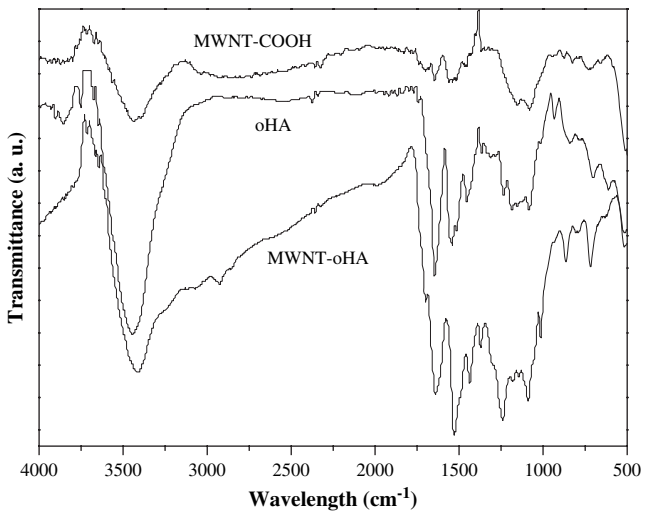

Fig. 3. ATR-IR spectra of MWNT-COOH, oHA, and MWNT-oHA.

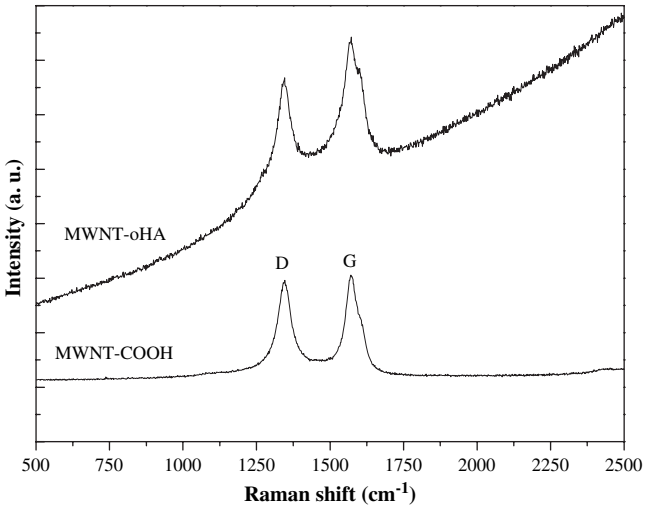

Fig. 4. Raman spectra of MWNT-COOH and MWNT-oHA.

thermal gravimetric analysis [15]. MWNT-oHA sample gives: C, 67.42; H, 3.15; N, 8.96. Given the weight composition of nitrogen atom of 10.98% in oHA, the weight composition of nitrogen atom of 8.96% in MWNT-oHA indicates that the weight compositions of oHA (ϕ_{oHA}) and nanotubes in MWNT-oHA are ~82 and ~18%, respectively. The degree of functionalization of MWNT with oHA can be calculated to be 32 using the equation of (ϕ_{MWNT}/carbon atomic weight)/(ϕ_{oHA}/oHA molecular weight). It means there is one oHA chain attached onto MWNT for every 32 MWNT carbon atoms. MWNT functionalized with –COOH or –COCl is ~3%, which is in good agreement with a previous report [14].

Both MWNT-COOH and MWNT-oHA have identical bands in their Raman spectra, shown in Fig. 4, despite a strong fluorescence for MWNT-oHA. It implies that the graphite structure of MWNTs largely remains after the functionalization, in agreement with earlier reports on MWNTs with carboxylic acid and acyl chloride groups [10,15]. As reported in the literature for MWNTs [15,20], the strong G doublet band at 1572 and 1600 cm^{-1} in the first-order Raman spectroscopy is the Raman-allowed phonon high-frequency first-order mode, and the disordered-induced D band at 1347 cm^{-1} can be ascribed to the defects in the curved graphene sheets, tube ends, and turbostratic structure of graphene [42,43]. Compared with the G bands generally observed at 1580 cm^{-1} for other carbon nanotubes [44], the downshift of G bands can be explained by the possible origins like different carbon nanotube specimens, laser illuminated positions, and incident laser power [15,45]. Although a higher integration ratio of D and G bands was reported to suggest more defects in MWNTs after functionalization [10,18], it is difficult to observe such a change in our results because of the strong fluorescence base line.

Fig. 5a and b shows the TEM images of entangled pristine MWNTs and a modified nanotube covalently bound with oHA layer, respectively. The average outer diameter of pristine MWNTs and MWNT-oHA can be estimated to be 25.9 ± 0.2 and 41.0 ± 0.2 nm. Therefore, the average thickness of enwrapped oHA layers can be roughly estimated to be ~7.5 nm. It was also found that a very small fraction of end-to-side hetero-junction structure exists in MWNTs-oHA as proposed for MWNT-oHA-MWNT at the bottom in Scheme 3. As discussed in an earlier report, such interconnected structures can be found in split bundles, where tube divergence occurs at various angles [46]. However, further studies need to be performed to confirm such "junction structure".

The solubilities of pristine MWNT, MWNT-COOH, and MWNT-oHA are summarized in Table 1. Pristine MWNT was insoluble in all tested solvents except MSA in which nanotubes were stabilized against aggregation by the formation of electrostatic double layers

Table 1
Solubilities of pristine MWNT, MWNT-COOH, and MWNT-oHA in various solvents

Sample[a]	H_2O	H_3PO_4	THF	DMAc	NMP	MSA
MWNT	–[b]	–	–	–	–	±
MWNT-COOH	±	–	–	–	–	±
MWNT-oHA	–	–	±	±	+	+

[a] THF, DMAc, NMP, and MSA denote tetrahydrofuran, dimethyl acetamide, *N*-methyl-2-pyrrolidone, and methanesulfonic acid, respectively.
[b] "–", "±", and "+" denote "insoluble", "partially soluble", and "soluble", respectively.

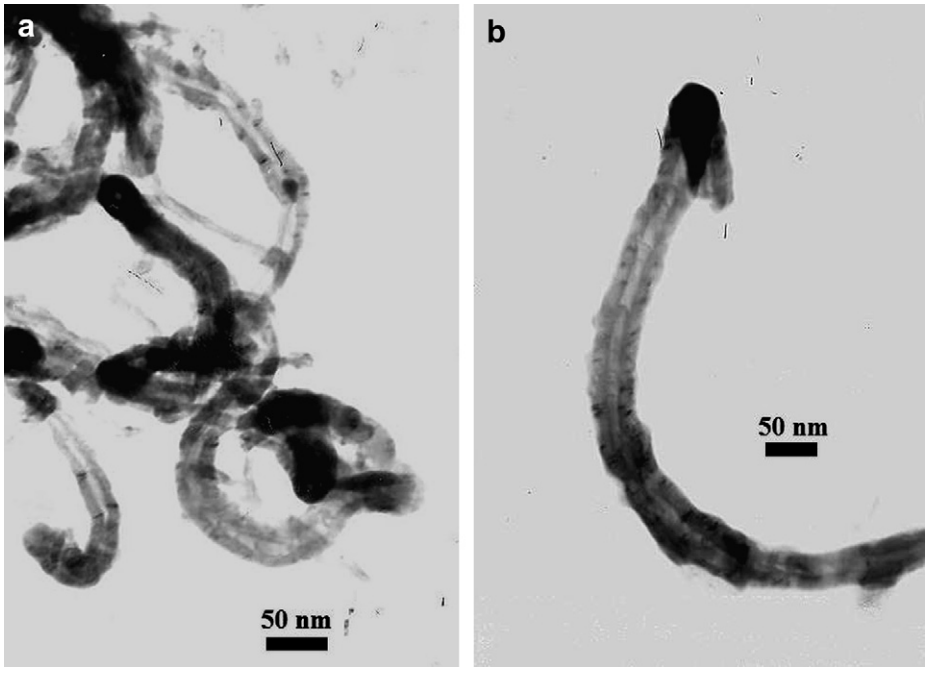

Fig. 5. TEM images of (a) pristine MWNTs and (b) MWNT-oHA.

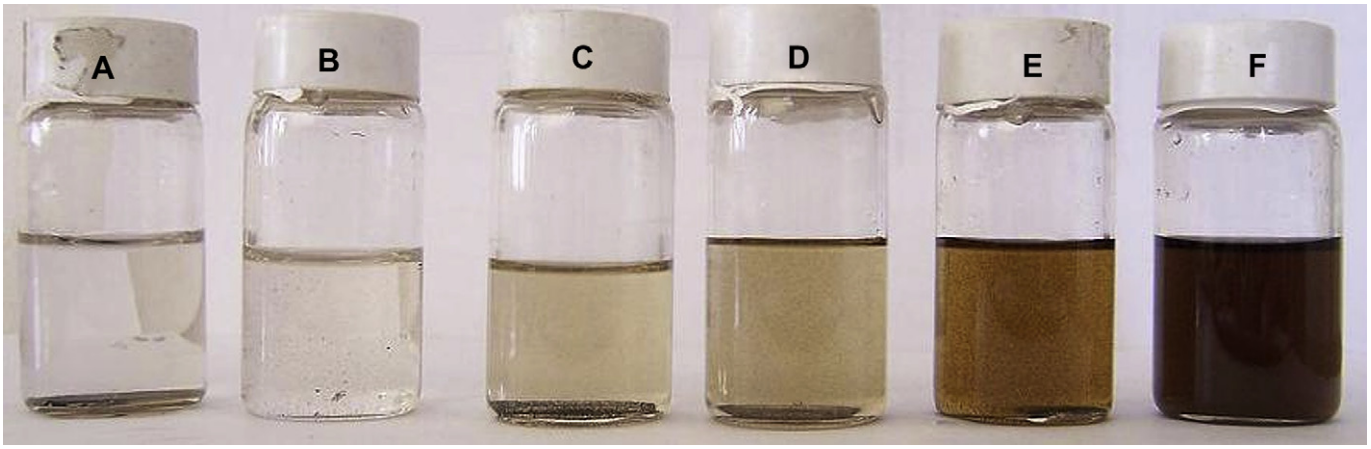

Fig. 6. Photograph of MWNTs-oHA placed in solvents (1.25 mg/mL) after one week (A: H_2O, B: H_3PO_4, C: THF, D: DMAc, E: NMP, F: MSA).

of protons and negative counter-ions [47]. After the oxidation of MWNTs with HNO_3, polar carboxyl groups were introduced onto the convex surface of MWNTs and therefore MWNT-COOH was partially soluble in water. Fig. 6 shows a photo of MWNTs-oHA placed in various solvents for 1 week. MWNT-oHA demonstrates certain solubility in polar solvents such as THF, DMAc, and NMP. Compared with MWNT-COOH, the solubility of MWNT-oHA in MSA is enhanced significantly, suggesting that oHA has been covalently grafted onto the carbon nanotubes.

Fig. 7 shows the TGA thermograms of MWNT-COOH, oHA, and MWNT-oHA. MWNT-COOH decomposes slowly with increasing temperature up to 800 °C likely because of losing carboxyl groups from the surface of MWNTs [15–22]. Oligo-HA shows two thermal degradation steps. The first degradation step occurs in the temperature range of 250–400 °C due to the loss of water in the hetero-cyclization of oHA, forming PBO. The weight drop of ~11 wt% in this temperature range is in good agreement with the calculated value of ~10 wt% for the weight loss of H_2O in the hetero-cyclization depicted in Scheme 4. The second degradation step for oHA at ~650 °C can be attributed to the thermal decomposition of formed PBO [23–29]. In the TGA thermogram of MWNT-oHA, there are also two inflections similar to those of oHA. Because there is less acylamide group in MWNT-oHA, the weight drop in the temperature range of 250–400 °C is ~9 wt%, slightly lower than that for oHA. The weight compositions of oHA and nanotubes in MWNT-oHA can be estimated from the weight drop of ~82 and ~18%, which are consistent with the elemental analysis discussed earlier. The second degradation step of MWNT-oHA is identical to that of oHA except a higher fraction of residue due to the existence of MWNTs. A predicted thermogram is made for the MWNT-oHA composite based on the compositions and also the weight drops for both components at different temperatures. The predicted dotted curve in Fig. 7 agrees with the experimental curve satisfactorily.

3.2. Structural characterizations of PBO–MWNT composite fiber

PBO–MWNT composites with MWNT compositions of 0.18, 0.36, and 0.54 wt% are named as PBO–MWNT (0.18%), (0.36%), and (0.54%), respectively. The intrinsic viscosities [η] for PBO, PBO–MWNT (0.18%), (0.36%), and (0.54%) in MSA at 30.0 ± 0.2 °C are 11.2, 10.9, 10.7, and 10.2 dL g^{-1}, respectively. It suggests that the molecular weight of PBO in the composites from in situ polymerization is almost as high as that of pure PBO. Using the Mark–Houwink–Sakurada (MHS) equation [28], the weight-average molecular weight M_w of PBO is calculated to be around 1.7×10^4 g mol^{-1}.

Fig. 8 shows the FTIR spectra of PBO and PBO–MWNT composite. The dehydrative cyclization of oHA to form a benzoxazole ring was confirmed by the disappearance of the broad absorption band at 3100–3400 cm^{-1} (not shown) for –OH and –NH groups and the strong band at 1650 cm^{-1} for amide I [23–27,29]. The characteristic peak at ~1720 cm^{-1} for PBO assigned to the stretching vibration of

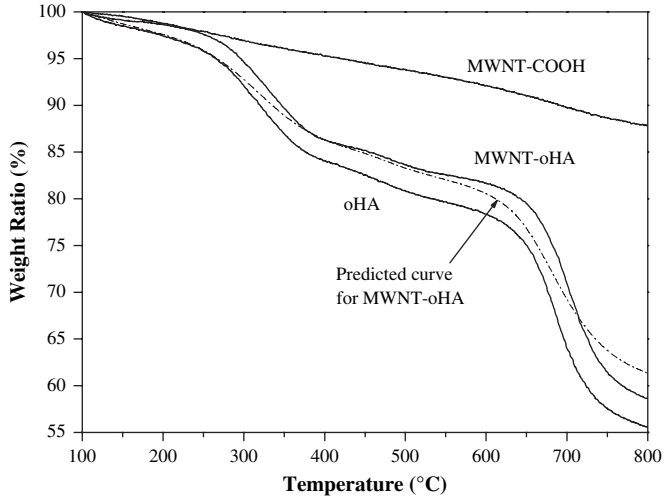

Fig. 7. TGA thermograms of MWNT-COOH, oHA, and MWNT-oHA with a predicted curve for MWNT-oHA.

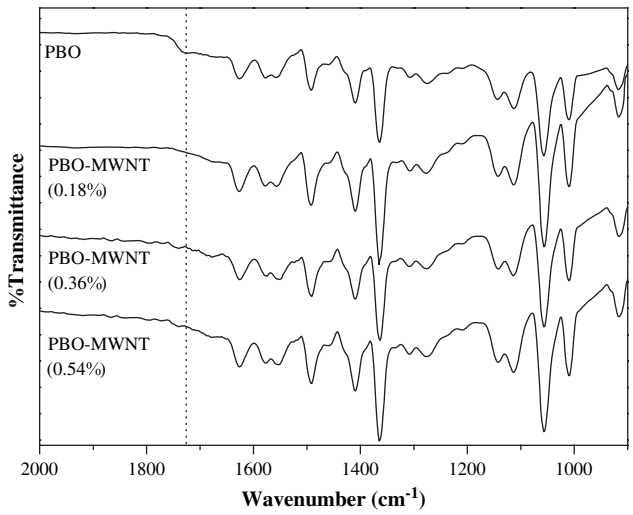

Fig. 8. FTIR spectra of (a) PBO, (b, c) PBO–MWNT (0.18%), (0.36%), and (0.54%).

–C═O in the end carboxylic groups diminished in the PBO–MWNT composites. It suggests that oligo-HA on the nanotube surface likely reacted with the end carboxylic groups of PBO in the in situ polymerization of nanocomposites, as proposed in Scheme 4. Moreover, the nanocomposites with different MWNT compositions display no distinguishable difference in most band positions from those of the polymer matrix due to the low compositions of MWNTs.

Heat treatment was found earlier to improve chain packing and orientation of rigid-rod polymer fibers, and consequently enhance their mechanical properties [35]. In the following discussion, PBO–MWNT composite fibers after heat treatment are named as PBO–MWNT HT fibers to distinguish from untreated fibers. WAXD patterns from equatorial and meridional scans of PBO, PBO HT, PBO–MWNT (0.54%) and PBO–MWNT (0.54%) HT fibers are shown in Fig. 9A and B, respectively. For PBO–MWNT fibers, diffraction peaks for MWNTs are not detectable in Fig. 9 and all the diffraction peaks can be assigned to the ordered structure of PBO in PBO–MWNT fibers [35–41]. The two diffraction peaks at $2\theta = 16.1$ and 26.5° correspond to the side-to-side and face-to-face *d*-spacings of 0.549 and 0.336 nm between two neighboring PBO chains on (200) and (010) planes, respectively [35]. It implies that the ordered structure of PBO matrix largely remains after adding MWNTs, as also found in PBO–SWNT fibers at much higher single-walled carbon nanotube (SWNT) compositions of 5 and 10 wt% [34].

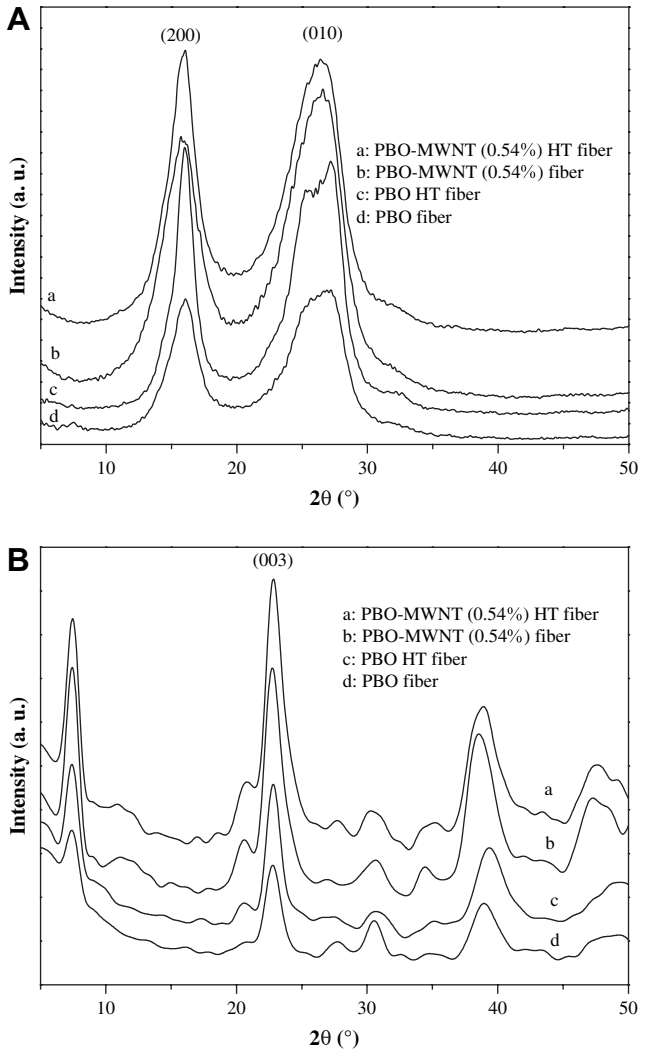

Fig. 9. Wide-angle X-ray diffraction patterns of (a) PBO–MWNT (0.54%), (b) PBO–MWNT (0.54%) HT, (c) PBO, and (d) PBO HT fibers in the equatorial (A) and meridional (B) directions.

Table 2
Apparent crystal sizes and orientation degree of PBO and PBO–MWNT (0.54%) fibers before and after heat treatment

Sample fibers	Apparent crystal size L_{003} (nm)	Apparent crystal size L_{200} (nm)	Orientation degree f_x %
PBO	12.1	8.2	87.8
PBO HT	12.4	8.6	89.5
PBO–MWNT (0.54%)	10.7	7.2	86.1
PBO–MWNT (0.54%) HT	11.1	8.4	87.0

The equatorial and meridional diffraction patterns reveal the intermolecular regularity between neighboring polymer chains and chain orientation degree along the fiber axis, respectively. Apparent crystal size (L_{hkl}) of PBO could be computed using Scherrer's equation,

$$L_{hkl} = K\lambda/B\cos\theta_{hkl} \quad (1)$$

where λ is the wavelength of the Cu Kα beam (1.54 Å), K is a constant of 0.89, and B is the half-width of the (hkl) reflection at a scattering angle $2\theta_{hkl}$. As listed in Table 2, apparent crystal sizes are obtained using Eq. (1) from the most prominent diffraction peaks (200) in equatorial direction and (003) in meridional direction.

After heat treatment, PBO–MWNT HT fiber shows slightly higher apparent crystal sizes of 8.6 and 12.4 nm in the equatorial and meridional directions, respectively, compared to 8.4 and 12.1 nm for its untreated counterpart. This phenomenon is similar to the intensified sharpness in the diffraction peaks for heat-treated polybenzazole fibers observed by our group [35] and Kitagawa et al. [48]. Meanwhile, the apparent crystal size of PBO–MWNT (0.54%) fiber also increases from 7.2 to 8.4 nm in the equatorial direction and from 10.7 to 11.1 nm in the meridional direction. It indicates that the heat treatment could improve the crystallization of the molecular chains [35,48,49]. The slightly lower apparent PBO crystal size in PBO–MWNT HT fibers than that in PBO HT fiber suggests that MWNTs are deleterious for the packing of PBO molecular chains.

The orientation degree of crystal was also analyzed from WAXD patterns. Azimuthal intensity distribution of the (200) diffraction was first achieved from two-dimensional imaging WAXD data (not shown). Then the orientation degree (f_x) of PBO and PBO–MWNT HT fibers can be calculated by the following empirical equation:

$$f_x = \frac{180 - H}{180} \times 100\% \quad (2)$$

where H is the half-width of the (200) peak estimated from curve-fitting. The orientation degrees of PBO and PBO–MWNT HT fibers are given in Table 2. Improved orientation of polymer chains can be observed after heat treatment as f_x increases from 87.8 to 89.5% for PBO fiber and from 86.1 to 87.0% for PBO–MWNT (0.54%) fiber. The lower increment in f_x in PBO–MWNT fiber compared with PBO fiber indicates that MWNTs incorporated with PBO backbone hinder the orientation of PBO chains.

SEM images in Fig. 10 demonstrate the morphology of both longitudinal outer surfaces and fracture surfaces of PBO and PBO–MWNT (0.54%) fibers before and after heat treatment. There are slight cracks or/and micro-fibrils on the fiber surfaces, which may be caused by the friction between fiber and spinneret and scoops in the process of spinning. The surface texture also reflects the uniformity of the coagulation process and subsequent fiber shrinkage due to the volume loss of the solvent PPA. It can be observed from Fig. 10a and c that the outer surface of the composite fiber is smoother than that of PBO fiber because MWNTs prevent polymer chains from fluctuation and rearrangement when coagulated in phosphoric acid and water. Meanwhile, the fracture of composite fiber in Fig. 10d is rougher than that of PBO fiber because of the

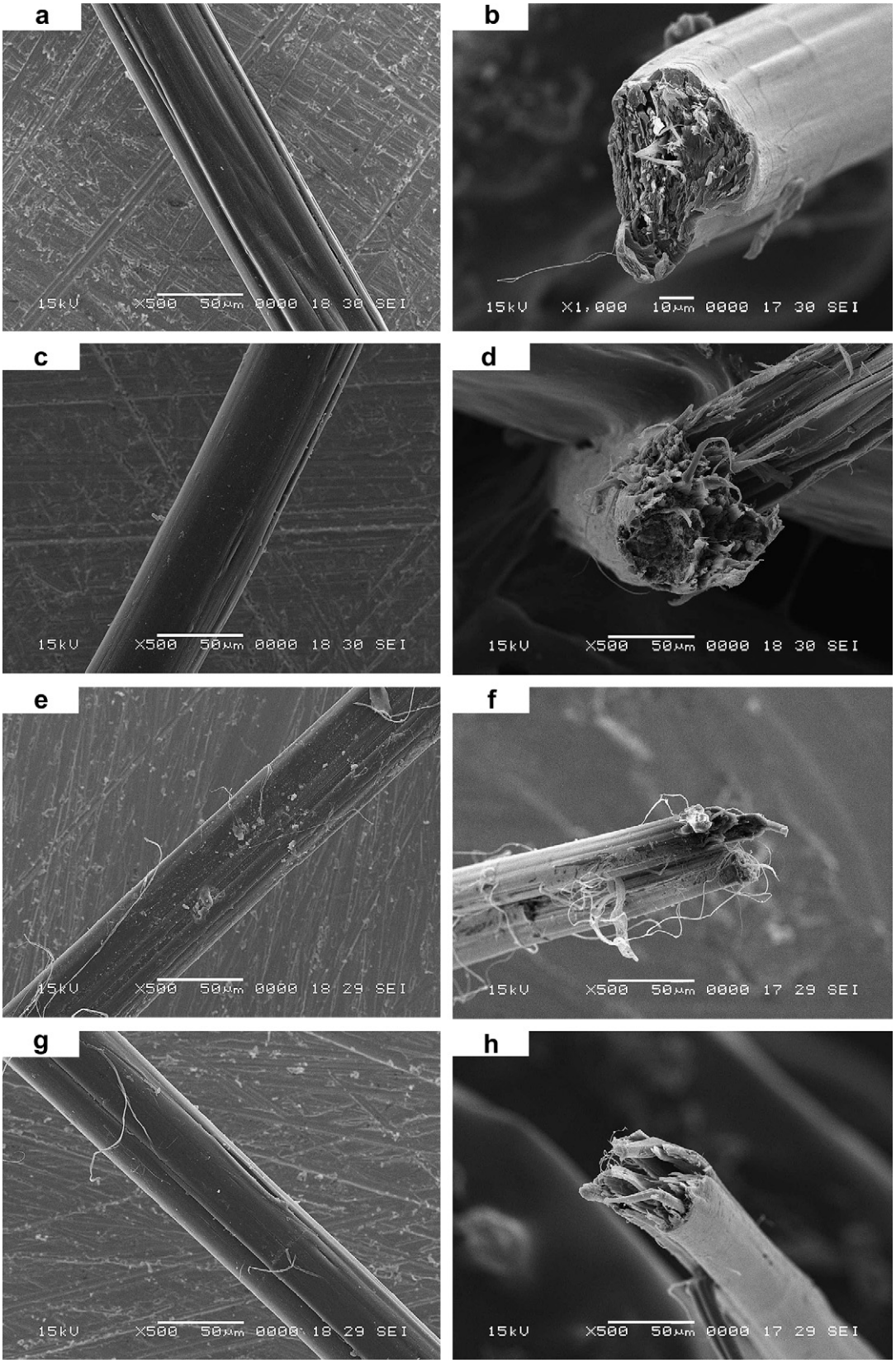

Fig. 10. SEM images of the longitudinal outer surfaces and fracture surfaces of (a, b) PBO, (c, d) PBO–MWNT (0.54%), (e, f) PBO HT, and (g, h) PBO–MWNT HT (0.54%) fibers.

existence of MWNTs and strong interfacial interactions between MWNTs and PBO matrix. After heat treatment, the fracture surfaces of both PBO and PBO–MWNT (0.54%) fibers become more compact and rougher, similar to our earlier observations on polybenzazole fibers [35] and polybenzazole/MWNT-COOH composite films [50]. Heat treatment could impel PBO molecular chains to adjust and slide along the fiber axis for further orientation, resulting in better-aligned PBO chains and a more regular structure. In addition,

MWNTs incorporated with PBO chains can be also aligned along fiber axis after heat treatment, which is beneficial for improving composite fibers' mechanical properties.

3.3. Physical properties of PBO–MWNT composite fiber

Table 3 lists the mechanical properties of PBO and PBO–MWNT fibers fabricated using dry-jet wet-spinning technique. PBO fibers show an average tensile strength of 1.18 GPa and an average tensile modulus of 66.6 GPa. After heat treatment, tensile strength and modulus increase to 1.22 and 89.8 GPa, respectively. Compared with the PBO fiber having a tensile strength of 2.6 GPa in an earlier report by Kumar et al. and the commercial PBO fiber (Zylon HM) having a tensile strength of 5.8 GPa [34,51], the relatively lower mechanical properties of the PBO fiber in this study is presumably due to a larger diameter of spinneret exit and a lower draw ratio for chain alignment. After the incorporation of MWNT-oHA with PBO matrix, tensile modulus and strength of the composite fibers increase moderately, making fibers tougher and more resistant to deformation. Since the orientation degree of PBO–MWNT fiber is lower than that of PBO fiber (see Table 2), the enhanced mechanical properties should be attributed to uniform dispersion and alignment of MWNTs in PBO matrix. Such dispersion benefits from both chemical bonding and physical interactions between nanotubes and PBO matrix.

After heat treatment, tensile modulus (or Young's modulus) and strength of PBO–MWNT fibers increase while the elongation at break decreases, as listed in Table 3. Consistent with our previous investigations on the polybenzazole fibers [35] and polybenzazole/MWNT-COOH films [50], such enhancements in tensile modulus and strength result from the improved microstructure of nanocomposite fiber and optimized interface between nanotubes and polymer matrix as discussed earlier. For comparison, PBO–MWNT-C HT fiber was prepared by polymerizing PBO with 0.57 wt% MWNT-COOH and heat-treated in the same condition as that for PBO–MWNT HT fiber. As shown in Table 3, tensile strength and modulus of PBO–MWNT-C HT fiber increase by 9.8 and 2.7% compared with those of PBO HT fiber. In contrast, PBO–MWNT HT fiber at an MWNT composition of 0.54 wt% results in enhancements of 23.8 and 11% in these two mechanical characteristics. These data are comparable to the results (23.1 and 13%) of PBO–SWNT composite fiber with a much higher SWNT composition of 5 wt% [34]. The significant enhancements at such a low CNT composition in PBO–MWNT HT fiber can be attributed to the improved compatibility between nanotubes and PBO matrix and maximized load transfer.

A rule-of-mixtures calculation was performed to estimate the MWNT alignment in the nanocomposite fiber based on the mechanical properties of PBO–MWNT composite fiber using the Halpin–Tsai equations for predicting composites' tensile modulus [4,52–54]. There are two equations with distinct assumptions with MWNTs aligned along the axial direction of the fiber (Eq. (3)), or MWNTs randomly distributed as a 3D network within the fiber (Eq. (4)) [4,52–54]. Both equations are stated as:

$$E_p = \left[\frac{1 + 2(l_{NT}/d_{NT})\eta_p V_{NT}}{1 - \eta_p V_{NT}}\right] E_m \tag{3}$$

where $\eta_p = \dfrac{(E_{NT}/E_m) - 1}{(E_{NT}/E_m) + 2(l_{NT}/d_{NT})}$, and

$$E_c = \left[\frac{3}{8}\frac{1 + 2(l_{NT}/d_{NT})\eta_L V_{NT}}{1 - \eta_L V_{NT}} + \frac{5}{8}\frac{1 + 2\eta_U V_{NT}}{1 - 2\eta_U V_{NT}}\right] E_m \tag{4}$$

where $\eta_L = \dfrac{(E_{NT}/E_m) - 1}{(E_{NT}/E_m) + 2(l_{NT}/d_{NT})}$ and $\eta_U = \dfrac{(E_{NT}/E_m) - 1}{(E_{NT}/E_m) + 2}$.

In the above equations, E_p is the tensile modulus of the composite fiber with MWNTs aligned along the fiber axial direction, E_c is the tensile modulus of the composite fiber with 3D randomly distributed MWNTs, E_m is tensile modulus of PBO matrix, E_{NT} is tensile modulus (1 TPa) [55–58] of MWNT bundle, l_{NT} and d_{NT} are average length (1.0 μm) and diameter (30 nm) of MWNT bundles

Table 3
Dimension and mechanical properties of PBO and PBO–MWNT composite fibers before and after heat treatment

Sample fibers	Diameter of fiber (μm)	Tensile strength (GPa)	Tensile modulus (GPa)	Elongation at break (%)
PBO	56 ± 2[a]	1.18 ± 0.05	66.6 ± 4	3.0 ± 0.3
PBO–MWNT (0.18%)	56 ± 2	1.23 ± 0.05	67.9 ± 4	3.1 ± 0.3
PBO–MWNT (0.36%)	58 ± 2	1.31 ± 0.05	69.0 ± 4	3.3 ± 0.3
PBO–MWNT (0.54%)	61 ± 2	1.48 ± 0.06	70.2 ± 4	3.9 ± 0.4
PBO HT	54 ± 2	1.22 ± 0.05	89.8 ± 5	2.3 ± 0.2
PBO–MWNT (0.18%) HT	55 ± 2	1.33 ± 0.05	93.7 ± 5	2.4 ± 0.2
PBO–MWNT (0.36%) HT	57 ± 2	1.42 ± 0.06	96.9 ± 5	2.5 ± 0.2
PBO–MWNT (0.54%) HT	59 ± 2	1.51 ± 0.06	99.8 ± 6	2.8 ± 0.3
PBO–MWNT-C HT[b]	56 ± 2	1.34 ± 0.06	92.3 ± 6	2.9 ± 0.3

[a] All the data are expressed as mean ± standard deviation.
[b] PBO–MWNT-C HT fiber was prepared by polymerizing PBO with 0.57 wt% MWNT-COOH in same condition as that for PBO–MWNT HT fiber.

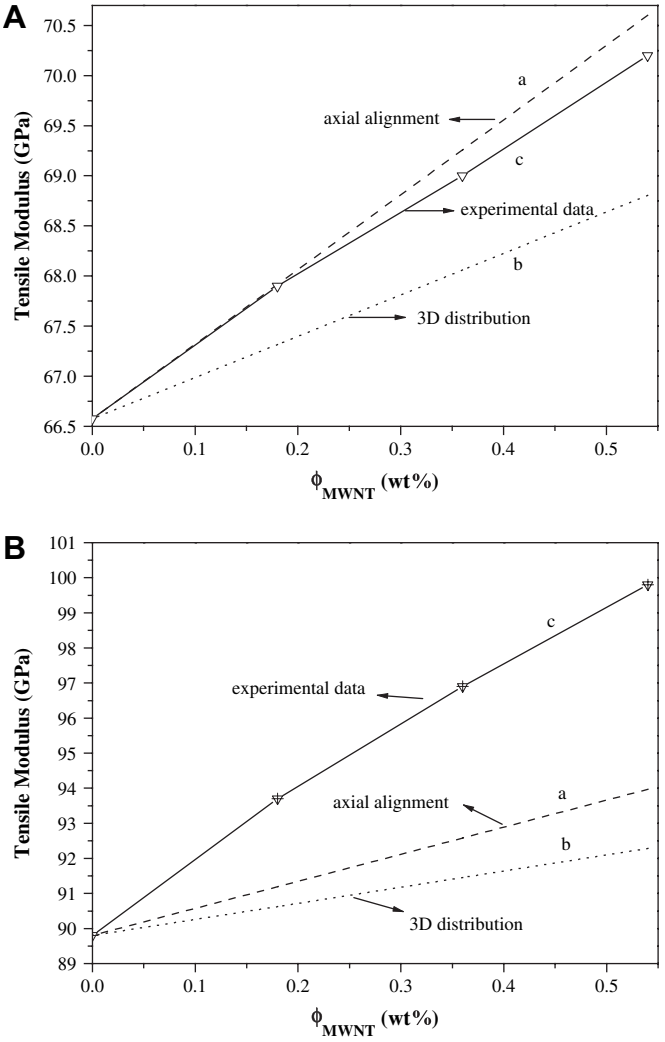

Fig. 11. Experimental data (c) of tensile modulus of (A) PBO–MWNT (0.54%) and (B) PBO–MWNT HT (0.54%) fibers compared with the predictions using the Halpin–Tsai equations based on two different assumptions: (a) MWNT aligned along the axial direction of the fiber; (b) MWNT randomly distributed as a 3D network within the fiber.

used in this study, V_{NT} is the volume fraction of MWNTs [52–54]. The density for MWNTs, PBO, and PBO HT used for calculating V_{NT} is 1.600, 1.540, and 1.560 g cm^{-3}, respectively [51,59].

Fig. 11A shows that the measured tensile moduli of PBO–MWNT fibers are very close to the theoretical predictions for the composites in which MWNTs are uni-directionally aligned along the fiber axis, indicating that MWNTs are highly aligned in PBO matrix. The enhancement in tensile modulus indicated by the slopes of those curves in Fig. 11 is much lower than those for other polymer–CNT composites such as Nylon 6–SWNT [52–54]. It can be attributed to the high modulus E_m for PBO matrix using the slope's theoretical meaning indicated in the square brackets in Eqs. (3) and (4). For heat-treated PBO–MWNT fibers in Fig. 11B, the measured elastic moduli are higher than the theoretical values from both Eqs. (3) and (4). It can be tentatively interpreted by the stronger interfacial interaction and higher degree of orientation for both PBO segments and bound MWNTs after heat treatment. The interfacial interaction is so effective in strengthening the composites that should not be omitted in the calculations.

As demonstrated in TGA thermograms in Fig. 12, all PBO and PBO–MWNT composite fibers exhibit excellent thermal resistance. The onset decomposition temperature in N_2 increases slightly from 627 °C for PBO to 630, 632, and 645 °C for PBO–MWNT (0.18%), (0.36%), and (0.54%), respectively. Correspondingly, the percentage weight loss at 800 °C decreases weakly from 30.2 to 29.5, 29.3, and 28.8%. In contrast with the TGA thermograms for oHA and MWNT-oHA shown in Fig. 7, there is no observable weight drop in the temperature range of 250–400 °C for the PBO–MWNT composite prepared using in situ polymerization, confirming that oHA attached on the surface of MWNTs indeed participated fully in the hetero-cyclization to form PBO. Consequently, a good interfacial compatibility between MWNTs and PBO matrix is expected to improve thermal stability and reduce flammability in air.

Recently we found that the conductivity of heat-treated PBO/MWNT-COOH 2D blend film with 5 wt% MWNT-COOH is eight orders of magnitude higher than that of heat-treated PBO film because of a lower percolation threshold resulting from the misalignment of carbon nanotubes [50]. The conductivities of heat-treated PBO/MWNT-COOH films with MWNT-COOH compositions up to 10 wt% are shown in Fig. 13 as open circles with a solid curve through them as a function of MWNT-COOH composition. In this study, electrical conductivity increases from 1.9×10^{-12} S cm^{-1} for heat-treated PBO film to 4.2×10^{-10} S cm^{-1} for the heat-treated PBO–MWNT (0.54%) composite film prepared using in situ polymerization. The data are shown as solid squares in Fig. 13 and almost

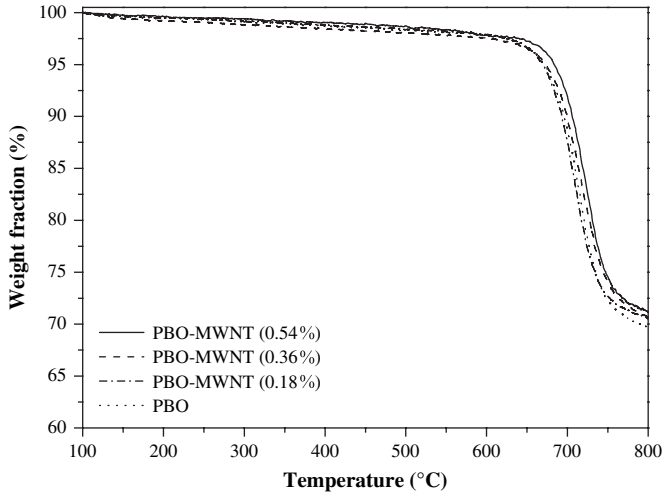

Fig. 12. TGA thermograms of PBO and PBO–MWNT (0.18%), (0.36%), and (0.54%).

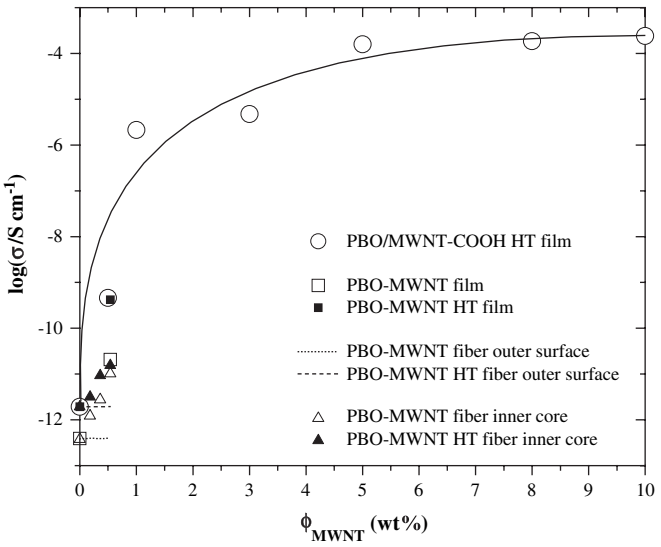

Fig. 13. MWNT weight composition dependence of electrical conductivity σ for PBO–MWNT composite fibers and films compared with the heat-treated PBO/MWNT-COOH blend films (open circles and solid curve).

identical to those for heat-treated PBO/MWNT-COOH films with the same MWNT compositions. Because PBO's conductivity is very low ($\sim 10^{-12}$ S cm^{-1}), the dominant contributor for conductivity is carbon nanotubes.

The DC electrical conductivity of PBO–MWNT fibers was measured on the outer surface of the fibers and the inner core of split fibers. Shown as the dotted horizontal line in Fig. 13, the outer surface of PBO–MWNT (0.54%) fiber shows a very low electrical conductivity of 3.9×10^{-13} S cm^{-1}, which is essentially identical to the value of PBO fiber. After heat treatment, all the conductivities increase to 1.9×10^{-12} S cm^{-1} while still no MWNT composition dependence can be found, shown as the dashed line in Fig. 13 in the MWNT composition range of 0–0.5 wt%. A similar phenomenon was also observed in PBO–SWNT composite fibers at a much higher SWNT composition of 10 wt% [34]. The lower conductivity in the outer surface of 1D PBO–MWNT composite fibers can be explained by the fact that well-dispersed and highly aligned small-fraction MWNTs exist in the polymer matrix and result in a much higher percolation threshold for forming continuous conductive channels [34]. As depicted in an earlier report by Winey et al. [60], the percolation pathway in the 2D nanocomposite films will be destroyed either at a MWNT-COOH composition lower than the threshold or in 1D PBO–SWNT fibers [34], in which preferentially aligned nanotubes seldom interact with each other to form a continuous conductive pathway along the fiber. The functionalization of the tubes should form a shell around the tube, increasing the distance that the tubes can approach to each other. Consequently, it will increase hopping/tunneling distance and decrease conductivity.

Surprisingly, a substantial increase in electrical conductivity with MWNT composition can be observed when the measurement was performed on the inner core of the split fiber, as shown in Fig. 13 using triangles. The conductivity of the fiber core without heat treatment increases from 3.77×10^{-13} S cm^{-1} for PBO to 1.22×10^{-12}, 2.73×10^{-12}, and 1.02×10^{-11} S cm^{-1} for PBO–MWNT (0.18%), (0.36%), and (0.54%), respectively. Similar to PBO–MWNT films, heat-treated fiber cores have higher values of 1.92×10^{-12}, 3.15×10^{-12}, 9.26×10^{-12}, and 1.55×10^{-11} S cm^{-1}, respectively. The higher conductivity and stronger MWNT composition dependence in the fiber core may imply that MWNTs are not evenly distributed over the cross-section of the composite fiber, or the fiber core differs from the skin in both morphology and chain alignment along the fiber axis. A recent investigation on the internal structure of PBO

fibers using on-axis scanning diffractometry revealed radial anisotropy or a skin-core morphology for the fibers with a more disordered or misoriented fiber core [61–63]. Consistently, a study on the morphology of polypropylene–nano carbon fiber composites discovered fewer carbon nanotubes with higher degree of orientation in the layer close to the fiber skin [64]. It is worthwhile to investigate further on the heterogeneous morphology for PBO–MWNT fibers from skin to core as well as the role of different morphology along the fiber axis in influencing electrical conductivity. Furthermore, insulate fiber skin and fairly more conductive core may suggest a potentially valid method to fabricate composite fibers to mimic cooper wires with insulate coating. Such conductive PBO–MWNT composite fibers will have excellent mechanical properties, outstanding chemical and thermal resistance, and a smaller density.

4. Conclusion

We have covalently functionalized MWNTs with oligo-hydroxyamide (oHA) via surface grafting of oHA onto the surface of MWNTs. Oligo-HA-functionalized MWNT (MWNT-oHA) prepared in this work contains ~18 wt% of MWNT and has a remarkable solubility in polar solvents. Oligo-HA has unique thermal degradation characteristics with two degradation steps, indicating the existence of benzoxazole ring closure to form a thermally more stable polymer PBO. PBO–MWNT composites with three compositions of MWNTs have been prepared through in situ polymerization of PBO in the presence of MWNT-oHA. PBO–MWNT composite fibers fabricated using dry-jet wet-spinning technique demonstrate improved tensile modulus, tensile strength, and thermal stability because of enhanced interfacial interaction of well-dispersed and highly-aligned MWNTs in PBO matrix. Increased electrical conductivity has been discovered in both PBO–MWNT composite films and the inner core of composite fibers although the outer surface of the fibers still shows no increase in conductivity upon adding MWNTs. This study explores the potential applications of covalently functionalized MWNT with oHA in reinforcing polymers and fabricating semi-conductive or anti-static articles.

References

[1] Iijima S. Nature 1991;354(6348):56–8.
[2] Ajayan PM, Zhou OZ. Appl Phys 2001;80:391–425.
[3] Baughman RH, Zakhidov AA, de Heer WA. Science 2002;297(5582):787–92.
[4] Bokobza L. Polymer 2007;48(17):4907–20.
[5] Coleman JN, Khan U, Blau WJ, Gun'ko YK. Carbon 2006;44(9):1624–52.
[6] Moniruzzaman M, Winey KI. Macromolecules 2006;39(16):5194–205.
[7] Niyogi S, Hamon MA, Hu H, Zhao B, Bhowmik P, Sen R, et al. Acc Chem Res 2002;35(12):1105–13.
[8] Ajayan PM, Schadler LS, Braun PV, editors. Nanocomposite science and technology. Weinheim: Wiley-VCH; 2003.
[9] Coleman JN, Khan U, Gun'ko YK. Adv Mater 2006;18(6):689–706.
[10] Wu T-M, Lin Y-W. Polymer 2006;47(10):3576–82.
[11] Hu GJ, Zhao CG, Zhang SM, Yang MS, Wang ZG. Polymer 2006;47(1):480–8.
[12] Oh S-J, Lee H-J, Keum D-K, Lee S-W, Wang DH, Park S-Y, et al. Polymer 2006;47(1):1132–40.
[13] Konyushenko EN, Stejskal J, Trchova M, Hradil J, Kovarova J, Prokes J, et al. Polymer 2006;47(16):5715–23.
[14] Haggenmueller R, Du F, Fischer JE, Winey KI. Polymer 2006;47(7):2381–8.
[15] Qin Y, Liu L, Shi J, Wu W, Zhang J, Guo Z-X, et al. Chem Mater 2003;15(17):3256–60.
[16] Kong H, Gao C, Yan D-Y. Macromolecules 2004;37(11):4022–30.
[17] Kong H, Gao C, Yan D-Y. J Am Chem Soc 2004;126(2):412–3.
[18] Park MJ, Lee JK, Lee BS, Lee Y-W, Choi IS, Lee S-G. Chem Mater 2006;18(6):1546–51.
[19] Ke G, Guan W, Tang C, Guan W, Zeng D, Deng F. Biomacromolecules 2007;8(2):322–6.
[20] Kuila BK, Malik S, Batabyal SK, Nandi AK. Macromolecules 2007;40(2):278–87.
[21] Lin Y, Zhou B, Fernando KAS, Liu P, Allard LF, Sun Y-P. Macromolecules 2003;36(19):7199–204.
[22] Lin Y, Rao AM, Sadanadan B, Kenik EA, Sun Y-P. J Phys Chem B 2002;106(6):1294–8.
[23] Kubota T, Nakanishi R. J Polym Sci Part B Polym Lett 1964;2(6):655–9.
[24] Akinseye TD, Harruna II, Bota KB. Polymer 1997;38(10):2507–13.
[25] Chang JH, Chen MJ, Farris RJ. Polymer 1998;39(23):5649–54.
[26] Kim T-K, Choi K-Y, Lee K-S, Park D-W, Jin MY. Polym Bull 2000;44(1):55–62.
[27] Schab-Balcerzak E, Jikei M, Kakimoto M. Polym J 2003;35(2):208–12.
[28] Wolfe JF. Polybenzothiazoles and polybenzoxazoles. In: Mark HF, Kroschmitz JI, editors. Encyclopedia of polymer science and technology. 2nd ed., vol. 11. New York: Wiley; 1988.
[29] Hsu SL-C, Chang K-C. Polymer 2002;43(15):4097–101.
[30] Kobashi K, Chen Z, Lomeda J, Rauwald U, Hwang W-F, Tour JM. Chem Mater 2007;19(2):291–300.
[31] Li X, Huang Y-D, Liu L, Cao H-L. J Appl Polym Sci 2006;102(3):2500–8.
[32] Li J-H, Chen X, Li X, Cao H, Yu H, Huang Y-D. Polym Int 2006;55(4):456–65.
[33] Huang J-W, Bai SJ. Nanotechnology 2005;16(8):1406–10.
[34] Kumar S, Dang TD, Arnold FE, Bhattacharyya AR, Min BG, Zhang X, et al. Macromolecules 2002;35(24):9039–43.
[35] Wang S, Wu P, Han Z. J Mater Sci 2000;35(23):5873–7.
[36] Wang S, Wu P, Han Z. Polymer 2001;42(1):217–26.
[37] Wang S, Wu P, Han Z. Macromolecules 2003;36(12):4567–76.
[38] Wang S, Guo P, Wu P, Han Z. Macromolecules 2004;37(10):3815–22.
[39] Wang S, Lei H, Guo P, Wu P, Han Z. Eur Polym J 2004;40(6):1163–7.
[40] Chen Y, Wang S, Zhuang Q, Li X, Wu P, Han Z. Macromolecules 2005;38(23):9873–7.
[41] Liu Z, Wang S, Zhuang Q, Li X, Li F, Wu P, et al. Chem Mater 2007;19(5):1164–9.
[42] Tan P, Zhang SL, Yue KT, Huang F, Shi Z, Zhou X, et al. J Raman Spectrosc 1997;28(5):369–72.
[43] Li W, Zhang H, Wang C, Zhang Y, Xu L, Zhu K, et al. Appl Phys Lett 1997;70(20):2684–6.
[44] Hiura H, Ebbesen TW, Tanigaki K, Takahashi H. Chem Phys Lett 1993;202(6):509–12.
[45] Ando Y, Zhao X, Shimoyama H. Carbon 2001;39(4):569–74.
[46] Chiu PW, Duesberg GS, Dettlaff-Weglikowska U, Roth S. Appl Phys Lett 2002;80(20):3811–3.
[47] Ramesh S, Ericson LM, Davis VA, Saini RK, Kittrell C, Pasquali M, et al. J Phys Chem B 2004;108(26):8794–8.
[48] Kitagawa T, Murase H, Yabuki K. J Polym Sci Polym Phys 1998;36(1):39–48.
[49] Pottick LA, Farris RJ. Polym Eng Sci 1991;31(20):1441–9.
[50] Zhou C, Wang S, Zhuang Q, Han Z. Unpublished results.
[51] Hu XD, Jenkins SE, Min BG, Polk MB, Kumar S. Macromol Mater Eng 2003;288(11):823–43.
[52] Gao J, Itkis ME, Yu A, Bekyarova E, Zhao B, Haddon RC. J Am Chem Soc 2005;127(11):3847–54.
[53] Yeh M-K, Tai N-H, Liu J-H. Carbon 2006;44(1):1–9.
[54] Thielemans W, McAninch IM, Barron V, Blau WJ, Wool RP. J Appl Polym Sci 2005;98(3):1325–38.
[55] Treacy MMJ, Ebbesen TW, Gibson JM. Nature 1996;381(6584):678–80.
[56] Falvo MR, Clary GJ, Taylor RM, Chi V, Brooks FP, Washburn S, et al. Nature 1997;389(6651):582–4.
[57] Wong EW, Sheeham PE, Lieber CM. Science 1997;277(5334):1971–5.
[58] Yu M-F, Lourie O, Dyer MJ, Moloni K, Kelly TF, Ruoff RS. Science 2000;287(5453):637–40.
[59] Chae HG, Kumar S. J Appl Polym Sci 2006;100(1):791–802.
[60] Du FM, Fischer JE, Winey KI. Phys Rev B 2005;72(12):121404.
[61] Davies RJ, Burghammer M, Riekel C. J Synchrotron Radiat 2005;12(6):765–71.
[62] Davies RJ, Burghammer M, Riekel C. Macromolecules 2005;38(8):3364–70.
[63] Davies RJ, Burghammer M, Riekel C. Macromolecules 2007;40(14):5038–46.
[64] Kumar S, Doshi H, Srinivasarao M, Park JO, Schiraldi DA. Polymer 2002;43(5):1701–3.